

Chapter 3

Related work

Since Wilhelm Roentgen discovered the existence of x-rays in 1895 [46], medical imaging has advanced at a tremendous rate, with x-rays, fluoroscopy, ultrasound, CT, MRI, positron emission tomography (PET) and single photon emission computerised tomography (SPECT) becoming fundamental diagnostic tools in modern healthcare. The developments in medical imaging technology are likely to advance into this century [109], in part due to the rapid advances in computer technology. At present, most systems do not directly utilise the acquired images, but instead rely on the subjective findings from a human observer. Therefore, in addition to the hardware improvements that will allow more accurate medical images to be acquired, there will undoubtedly be further progress on computer aided diagnosis and computerised decision support in medical imaging.

Computers have been used in medical imaging for many years, with their initial application focusing purely on administrative functions. Early radiology information systems (RIS) were developed in the 1970s for billing and patient registration. Nuclear medicine was the first specialty to actually utilise computers in imaging, closely followed by digital subtraction angiography (DSA) for interventional radiology. Both CT in the 1970s and MRI in the 1980s relied on computers to reconstruct medical images from the raw collected data. In the late 1980s PACS became more common, replacing the traditional hard-copy based methods of managing medical images. Today, most hospitals are becoming increasingly more reliant on both RIS and PACS for both patient management and digital medical imaging [11].

Currently, two of the most popular areas of two-dimensional medical imaging research are computer-aided diagnosis (CAD) of breast lesions from mammographic images and automatic segmentation of medical images using deformable models. CAD has the potential to be a useful tool for the radiologist, by drawing attention to particular findings on the image, highlighting changes from previous images, or quantifying the size, shape and texture of features. Some CAD systems are used for image registration, virtual interaction, visualisation, simulation or training. At present CAD is used for the identification of clustered microcalcifications and masses in breast tissue, that are visible on a mammogram [28]. These systems are reportedly already capable of detecting possible malignant tumors with greater accuracy than most radiologists and equal to that of the best mammographers [11]. The number of false positives is still high, but according to Arenson et al. [11], having the system call attention to possible abnormalities is as good or better than a reading by a second radiologist. They also suggest that this type of aid could help reduce the variability in detecting abnormalities.

Interpretation of any medical image is a difficult problem, because a non-trivial algorithm will utilise some kind of automated system to understand the information contained within the image. Automated detection of fractures in x-ray images is one such problem. In some cases the general shape, orientation or location of the object of interest is known, and can be used to constrain a model so that analysis can take place. However in many cases this information is unknown, complicating the analysis greatly. While there have been attempts to solve many medical image analysis problems, very few of them have involved automated fracture detection. This chapter examines some published methods for automatically detecting fractures, as well as some relevant bone segmentation methods.

3.1 Computer aided diagnosis

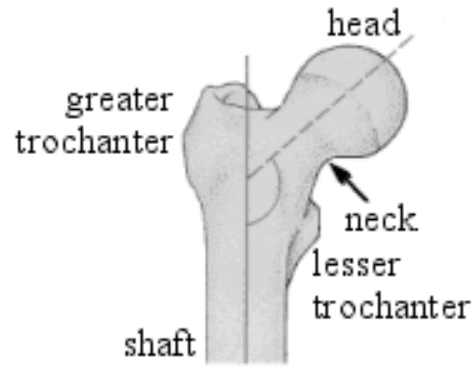
There is very little literature related to computer aided fracture detection, but some relevant work has been performed on detection of osteoporosis and bone age estimation. Of most interest is the work initiated by Tian et al. [105], who have created a computer

algorithm to detect femur and radius fractures.

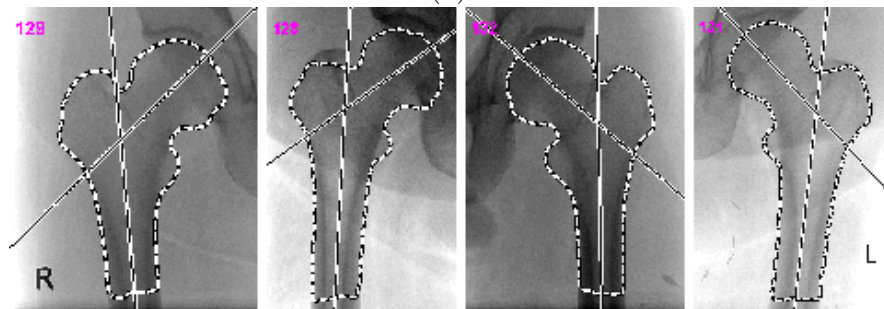
3.1.1 Femur and radius fractures

The method outlined by Tian et al. [105] detects femur fractures by computing the angle between the axis of the neck of femur, and the axis of the shaft. This measurement is made in three stages. The first involves extraction of the femur contour, the second involves the measurement of the neck-shaft angle (NSA, shown in Figure 3.1a), and the third is a classification of the measured angle. Extraction of the femur contour is not described in detail, but is said to be performed using Canny edge detection, Hough Transform, and active contours. Testing of this algorithm in [110] showed that the fracture detection rate was 61.5%. The results show that this method was only capable of detecting severe femur fractures that caused significant changes in the angle between the neck and the shaft. In many cases the neck of femur was fractured without displacing or rotating the head, and the resulting local disruption to the trabecular pattern was not detected. An example showing the results for both fractured and unfractured femora is shown in Figure 3.1b and c.

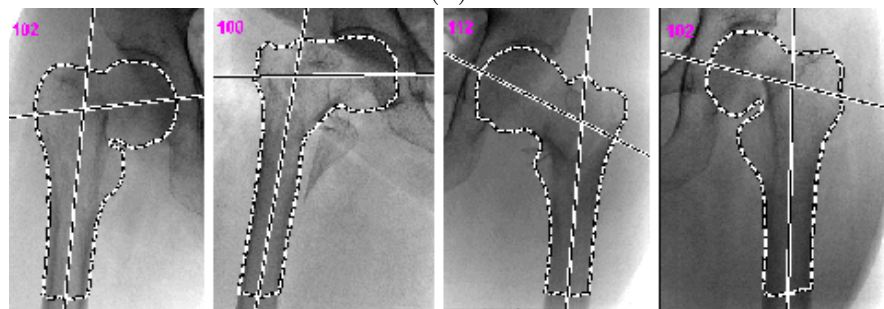
To overcome the problems that resulted from only measuring macroscopic changes to the bone, Yap et al. [110] developed a complementary method of detecting femur fractures, involving analysis of the disruption to the trabecular patterns present in the femoral neck. Their method also consisted of three stages, the first of which extracted the femur contour, the second analysed trabecular texture, and the third performed classification. To extract the femur from the image they used an active shape model—a snake (Section 3.2.1 on page 42) with gradient vector flow [104]—that was supplemented with active appearance models at distinct feature points. The anatomical structure of the bone in the neck of femur permits fracture detection by analysis of trabecular orientation, since these type of fractures cause significant disruption to the texture pattern. The dominant orientation of the texture is determined at a series of sampling locations within the femoral head using a set of Gabor filters (shown in Figure 3.2a and b for unfractured and fractured femora), referred to as Gabor orientation (GO) maps. Classification was performed using both a Bayesian classifier and Support



(a)



(b)



(c)

Figure 3.1: (a) Measurement of the femoral neck shaft angle (NSA), with (b) unfractured examples, and (c) fractured examples. Replicated from Tian et al. [105].

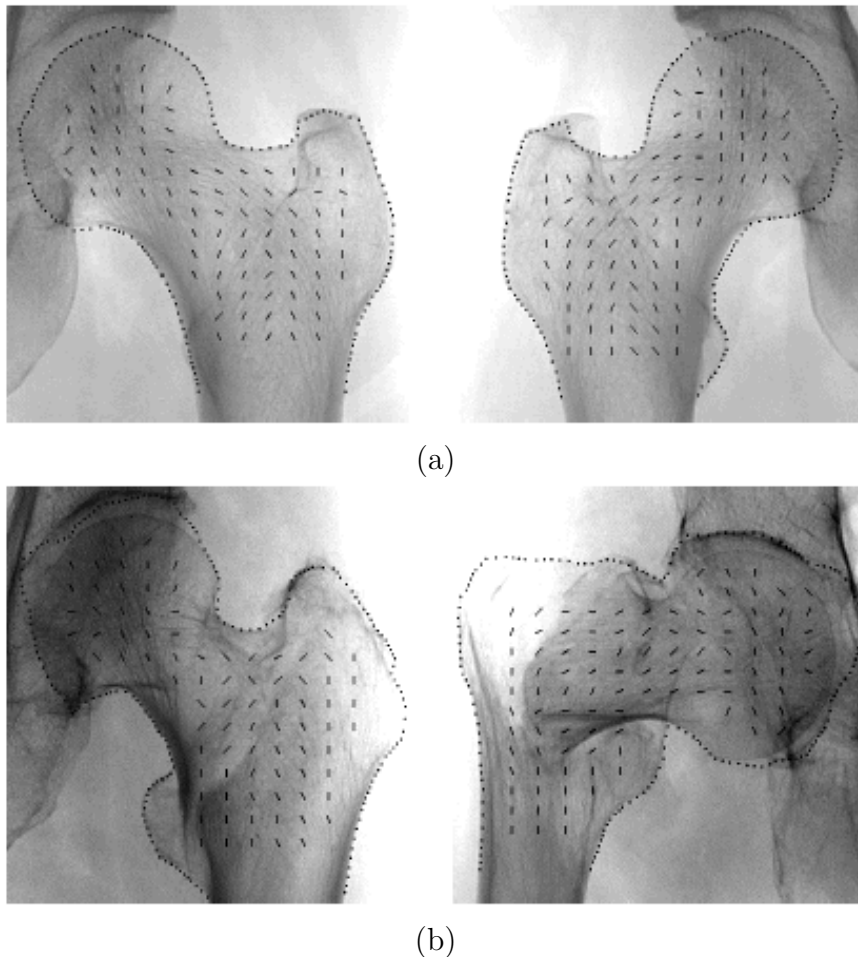


Figure 3.2: Gabor texture orientation maps of (a) unfractured and (b) fractured femora. Replicated from Yap et al. [110].

Vector Machine (SVM). The femoral neck was classified as fractured if either of the two classifiers or the NSA method classified it as fractured. This yielded a detection rate of 84.6%. While this method produced good results, it is only suited to the femoral neck, and cannot be adapted to other bones. Both methods also require a large amount of manual interaction, since segmenting the femoral neck typically requires a dozen initialisation points for the active contour.

A further refinement of these methods was undertaken by Lim et al. [59], who modified the feature extraction stage of the algorithm to include Markov Random Fields (MRF) and intensity gradient direction (IGD) to the existing method of NSA and GO maps. The classification methods in [110] were unmodified. If any two of the six classification methods were positive then the bone was classified as fractured. This produced an improved fracture detection rate of 92.2%, with a false positive rate of 1%. They also showed that the fracture detection rate of individual classifiers is not very high,

but they can be used to complement each other to give significantly improved classification accuracy. When tested on images of the radius, this same method produced a fracture detection rate of 82.6% with a false positive rate of 17.6%. Normal structures such as growth plates were often falsely classified as fractures. Finally, Lum et al. [65] improved the detection accuracy and sensitivity by combining classifiers. The three texture features utilised were again GO, MRF and IGD. This time, classifiers were combined using a number of rules such as max, min, sum, product, majority vote and the simple m -of- n (including OR and AND). They concluded that the OR rule (1-of- n) had the highest sensitivity and comparable accuracy.

3.1.2 Osteoporosis

Most research involving the analysis of orthopaedic x-ray images has been focussed on detecting osteoporosis and determining fracture risk, using methods such as texture and fractal analysis. Some groups [40, 63, 80] have used first order statistics such as the standard deviation and mean to measure texture, while others [71, 107] computed second order texture statistics like the co-occurrence matrix. Other methods such as surface area measurement [24], semi-variance [55] and power spectral analysis to determine the fractal dimension [23] have also been used to detect osteoporosis. Caligiuri et al. [24] found that in some cases their method was capable of distinguishing fractured specimens from normal specimens. Fractal analysis was applied to the micro x-ray images of human knees by Lynch et al. [66], while a multi-resolution wavelet technique was used by Matani et al. [70] to analyse the micro x-ray CT images of rat lumbar vertebrae. While this work is related, both used micro x-ray images rather than normal diagnostic x-rays.

3.1.3 Bone age estimation

In pediatrics, bone age estimation (BAE) is an important application of hand radiography, especially for the diagnosis of growth disorders and endocrinological problems [39]. A comparison of chronological age and skeletal age can indicate atypical skeletal development, as well as serve as an indication of any therapeutic effects of treatment.

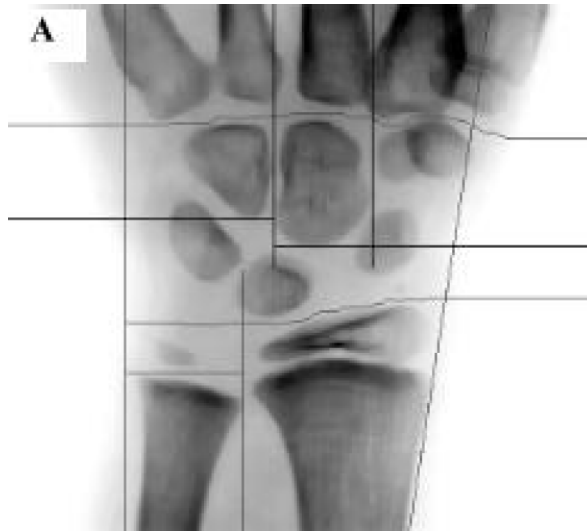


Figure 3.3: Carpal-bone region of interest division, to which the classifier is applied to determine bone age. Replicated from Fan et al. [39].

Skeletal maturity of a child can be determined from a standard radiograph of the ossification centres in the left hand and wrist, using one of a number of established clinical methods [78], including the Tanner and Whitehouse method, and the Greulich and Pyle method [74]. In the Tanner and Whitehouse method, 20 regions of interest in the hand are considered. The development of each region is classified into discrete stages, and given a numerical score. The sum of scores for all the regions produces a maturity score. The Greulich and Pyle method requires the comparison of all the bones in the hand and wrist against reference radiographs at different ages. Bone age estimation is a very subjective process, so the results are highly dependent on the expertise and experience of the assessor [39]. Like automatic fracture detection, automatic skeletal age assessment can potentially reduce the time required to examine an image, and also produce better repeatability.

To automatically determine bone age, Fan et al. [39] uses carpal bone features that are extracted using a 2-stage edge detection method, as well as a projection based method for determining the carpal bone region of interest (shown in Figure 3.3). The extracted features are applied to three classifiers, weighted minimum distance, Bayes, and a neural network. The Bayes and neural network classifiers produced the best results with an accuracy of over 90%, with best results occurring with children under the age of seven. In contrast, Niemeijer et al. [78] constructed mean images for each of the Tanner and Whitehouse regions (Figure 3.4a), and then trained an active shape

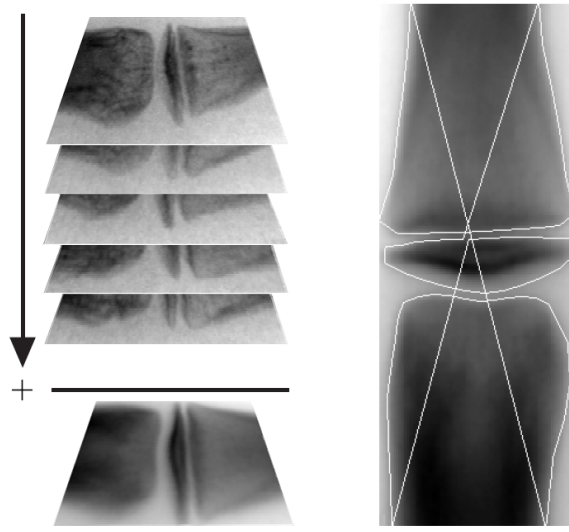
model to segment these regions in the input image (Figure 3.4b). The mean images were then aligned to the segmented regions using Procrustes analysis (Figure 3.4c), and the correlation between the two was calculated to produce a region score. Either the highest correlation is used to determine the maturity score, or the values are used as features and a classifier was trained to determine the score. The accuracy was stated to be 73%. The method relies on accurate segmentation of the bones by the active shape model. In a number of cases the segmentation is poor (right side of Figure 3.4b) because some natural anatomical variations do not match the model.

3.1.4 Non-visual fracture detection

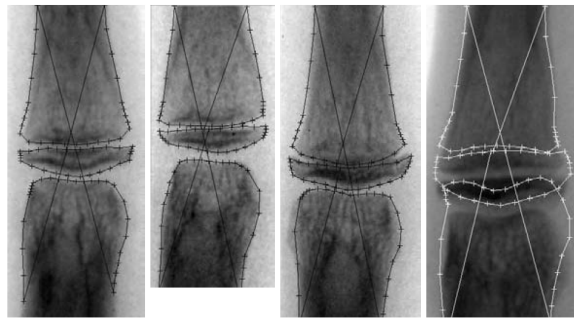
Other groups have attempted to detect fractures using non-visual techniques. Ryder et al. [91] analysed acoustic pulses as they travelled along a bone to determine if a fracture was present, Kaufman et al. [54] analysed mechanical vibrations in a bone using a neural network model, and Singh and Chauhan [96] measured electrical conductivity. Unfortunately none of these techniques are as accurate as x-rays for the diagnosis, localisation and classification of long-bone fractures, and as a result they are not used in a clinical setting.

3.2 Automatic image segmentation

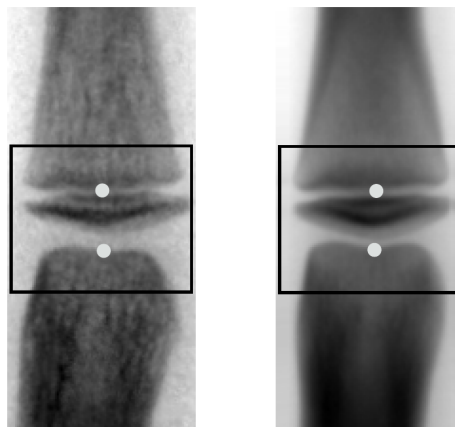
As mentioned throughout Section 3.1, the extraction of features from the image is a significant problem. This is because the anatomical structures present within medical images are generally very complex, both inter- and intra-subject variability is enormous, and the data sets are generally very large. In addition noise, sampling artifacts and spatial aliasing can cause the boundaries of the structures of interest to become indistinct or disconnected, so it is often a challenge to extract boundary elements belonging to the same structure [73]. Traditional low-level image processing techniques that consider only local information can make incorrect assumptions during the segmentation process and generate infeasible object boundaries. For many applications a complete and accurate segmentation is essential, however many systems either suffer from poor results, or require expert human intervention [34]. The accurate identifica-



(a)



(b)



(c)

Figure 3.4: (a) Calculation of a mean image for a particular stage by orthogonal projection. (b) Some examples of the segmentations performed using their active shape model (ranked from best to worst). (c) Correlation of the identified points in the query image (L) and the mean image (R) is used to determine the bone age. Replicated from Niemeijer et al. [78].

tion and segmentation of bones from a digital x-ray image is a necessary step for the automatic detection of fractures and other abnormalities. A number of groups have been working on different methods of automatically segmenting and identifying various bones from medical images. This section gives a very short and general introduction to deformable models, and demonstrates their use on a sequence of medical images. It also examines the relevant work that has been performed on segmenting the vertebrae, the bones in the arm and other long-bones, as well as other anatomical structures.

3.2.1 Deformable models

Many structures have been semi-automatically segmented from medical images using deformable models, such as geometric active contours, otherwise known as “snakes”. A deformable model is active in the sense that it can adapt itself to fit the given data. It is a useful shape model because of its flexibility, and its ability to both impose geometric constraints on the shape and to integrate local image features. Given an input image, the objective is often to produce complete and accurate contour line of a specific object within the image. A simple pixel-based identification is not satisfactory since a full mathematical and analytical description of the contour lines is desired.

The snake is an iterative algorithm first proposed in Kass et al. and Terzopoulos et al. [53, 101, 102] that can produce a good contour-line description. The current iteration of the algorithm receives as input the previous contour line and uses some balancing constant factors to produce a new contour line representation. Two forces are measured, an internal force that estimates the length and smoothness of the line (lower values produce a smoother and shorter line, forcing the contour inwards), and an external force from the gradient of the image pixel intensity (so major changes in the output values occur when the coordinates are close to the edges of the desired object). Iteratively minimising the resulting potential energy function produces the best estimate of the real contour. Since the use of non-geometric function parameters can cause the absence of a minimum value, or dual values, geometric parameters are used. A level set approach can be used to solve this problem, although it does not produce a meaningful analytic solution. This can be obtained by combining these

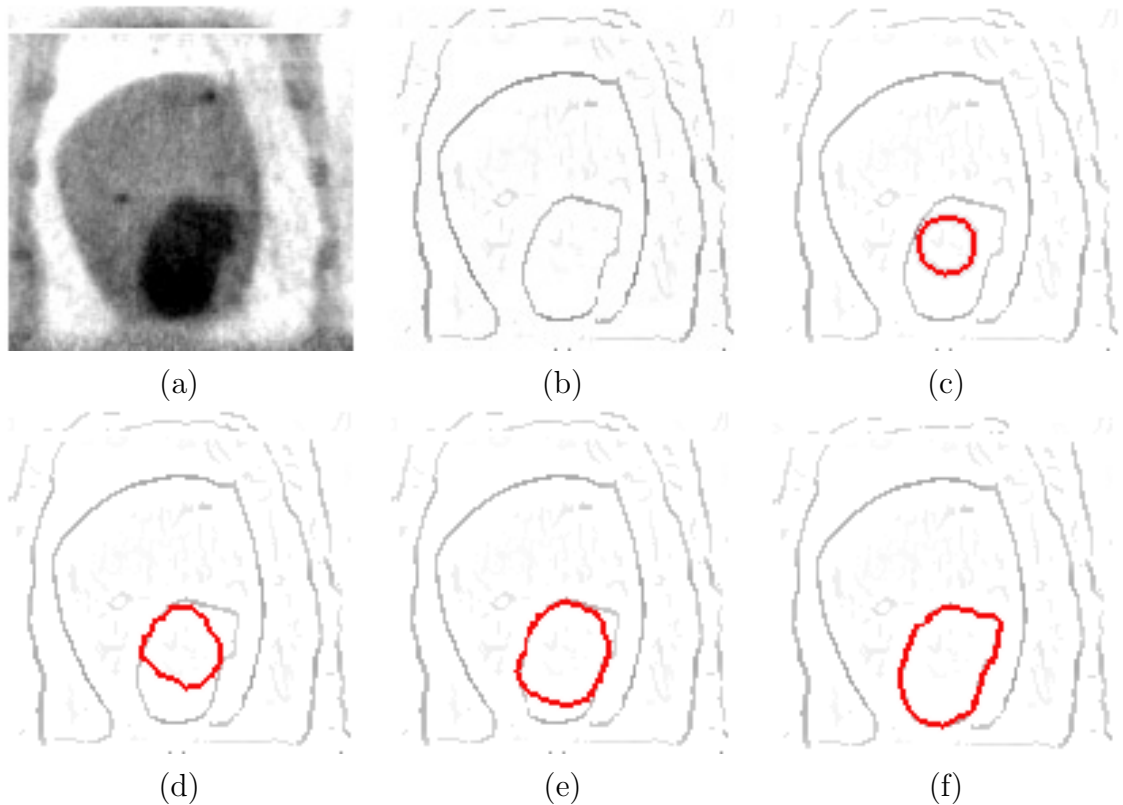


Figure 3.5: Active snake deformation. (a) Intensity CT image slice of the left ventricle. (b) The edge detected image. (c) The initial snake. (d-e) The snake deforming toward the ventricle boundary, driven by the inflation force. (f) The final contour matches the ventricular wall. Adapted from McInerney and Terzopoulos [73].

two concepts, which is termed geodesic active contours. An example showing the left ventricular segmentation produced by the snake model is shown in Figure 3.5.

This snake model provides a powerful interactive tool for image segmentation. However it uses strictly local information, so the original implementation is vulnerable to image noise and the initial position of the snake. In the literature, many provisions have been made to improve the robustness and stability of the snakes. Some of these [31] allow the snake to trespass spurious isolated weak image edges, and counter its tendency to shrink. This produces a snake that is more robust to the initial position and image noise, but human intervention is needed to decide whether an inflationary or deflationary force is needed. In addition, deformable models also require manual intervention to set the initial contour line that is to be deformed, often a difficult image processing task in itself. Nevertheless, active contours have been successfully extended to perform tasks such as edge and subjective contour detection, motion tracking, stereo matching and image segmentation. Indeed, some of the applications in the following

sections utilise active contours for segmentation tasks.

3.2.2 Vertebrae

Determining the location of the cervical vertebrae in x-ray images is an important problem that has been addressed by Tezmol et al. [103]. A robust segmentation method that utilises the generalised Hough Transform is used to find estimates of the location and orientation of the cervical vertebrae, independent of the image scale or rotation. Their customised approach to the generalised Hough Transform identifies objects based on shape, and exploits the shape information embedded in the Hough domain so that the effects of noise and occlusions are minimised. The generalised Hough Transform is a template-based technique that searches the target image for instances of the previously defined template. The use of multiple templates to capture the variability in shape is ideal, but the use of a collection of templates is very computationally expensive. Therefore the authors found the mean of 50 template images, to create a single template that best represents the target. Peak detection in the accumulator space then yields the spatial coordinates, scale and angle of rotation of the best matches to the template.

Landmark points were placed on the image by a radiologist (Figure 3.6), and the algorithm was tested against this by placing a bounding box at the site of the best template match. Using their proposed technique, an average of 72 out of 80 landmark points fell inside the bounding box, and the average orientation error was 4.16 degrees. However, the bounding box is very large, and its placement does not appear to be specific. Identification of fractures within the bounding box would certainly be a worthwhile, but as yet undocumented, task.

3.2.3 Tubular structures

There has been a substantial amount of work on the computer assisted radiological detection of tubular structures, such as lung bronchi and blood vessels, much of which has been performed using deformable models [76]. These models are well suited to repetitive tasks that are not necessarily difficult to perform manually, but are often relatively time consuming. Such tasks include automatically following and segmenting



Figure 3.6: The detected cervical vertebrae. Replicated from Tezmol et al. [103].

blood vessels through three-dimensional CT or MRI image slices, or tracing vessels in angiographic images. In these cases it is not difficult to manually draw the initial contour, and then allow it to deform to fit the structure of interest, thus substantially reducing the manual segmentation time. For large structures like long-bones, that contain a complex internal texture and a complex projected two dimensional shape, these methods will not necessarily produce good results, and since manual setup is usually required, fully automatic segmentation is difficult to achieve.

3.2.4 Arm fractures

The segmentation of fractured bones within an x-ray image of a patient’s arm is outlined by Jia and Jiang [51]. They utilise a geodesic active contour model with global constraints to identify bones within the arm. This procedure involves collecting a prior shape that is to be detected, and using this as the global constraint within the model. This allows the model to evolve toward the desired shape, and to register with the prior shape. To determine how good the fit is, a maximum-likelihood function is derived, and provides feedback at each step of the evolution.

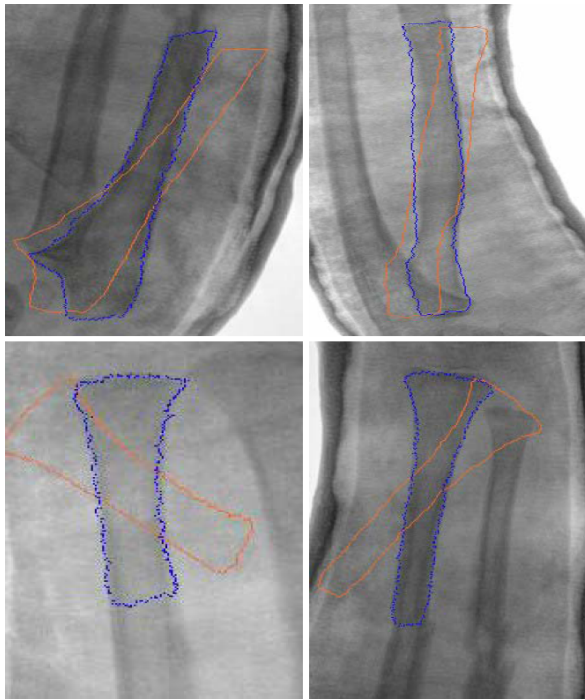
Jia and Jiang [51] state only that they have tested their algorithm on “more than 10 cases”, and that their results showed that their algorithm is “robust and accurate”, however without additional information their results are hard to quantify. Nevertheless,

an example of their work is shown in Figure 3.7. The initial position of the evolving curve is shown in orange in Figure 3.7a. The curve was allowed to evolve until the energy of the evolving function was minimised, and the result is shown in purple. Figure 3.7b shows their “bone alignment calculation result”, although no details were provided within the text about how this is achieved, or how well their method performs.

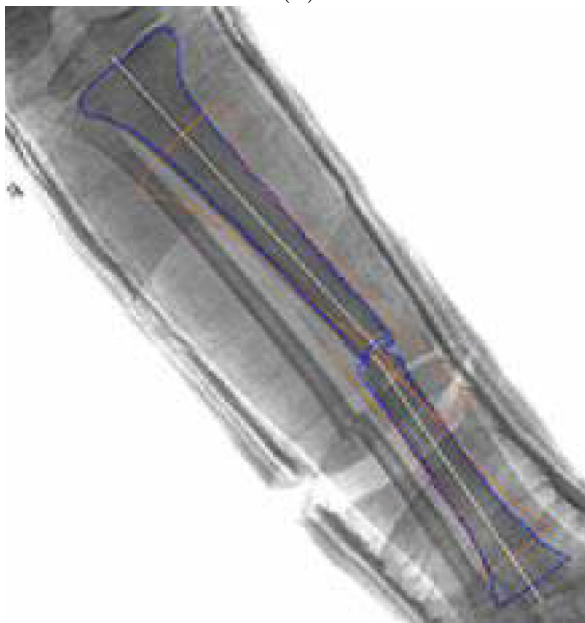
One major advantage of their method is that it can be used when the arm is covered by a casting material that typically interferes with the segmentation by reducing the signal to noise ratio, although it is not clear if the other described methods would also perform well in this situation. The major drawback with this method is that it requires a prior shape that must be very similar to the shape to be detected. By examining Figure 3.7a, it is possible to see that the prior shape and final evolution are essentially identical, other than their rotation about the centroid of the shape. Of course, it is often impossible to know the prior shape without first performing a manual segmentation, as has most likely been done in this case. Therefore this method would have extremely limited real world applications, as it presumably requires an accurate prior shape, as well as relatively precise placement of the prior shape within the image.

3.2.5 Long-bones

A model based bone segmentation method, specifically designed for long-bones is outlined by El-Kwae et al. [38]. Like the bone age estimation method described by Niemeijer et al. [78] in Section 3.1.3, their model is based on the knowledge of statistical variations in anatomical data that were collected by analysing diverse bone shapes. A bone is then modelled as two centroid points that correspond to each of the epiphyses, with a range of weighted values for the distances between the centroid and the boundary. For a positive match (Figure 3.8), a strong edge belonging to the boundary of the shape should be present within the calculated ranges. No results for their work are presented, however their model shows a huge amount of anatomical variation, that would most likely reduce the precision of any match. In addition, they also only show detection of a single long-bone within an image, without any subsequent segmentation. No other solutions to the problem of fracture detection in long-bones were found.

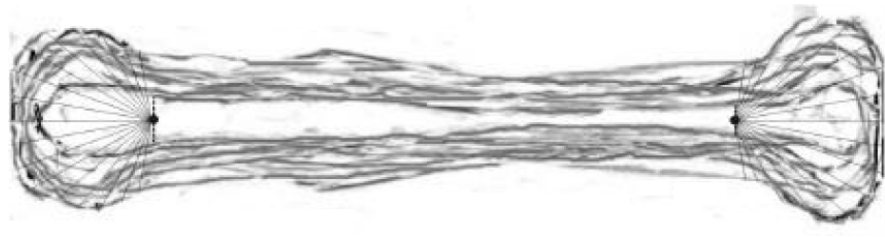


(a)

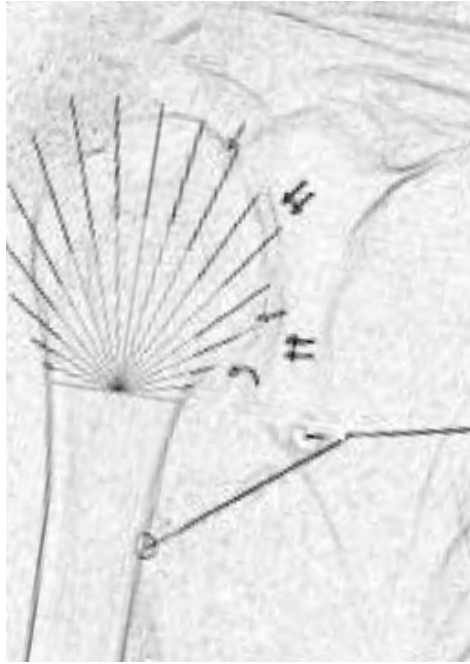


(b)

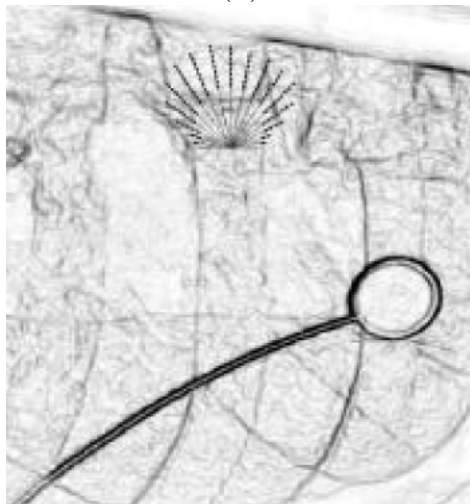
Figure 3.7: (a) Experimental results, in which the initial curves are shown in orange, and the final results in purple. (b) Their bone alignment calculation result. Replicated from Jia and Jiang [51].



(a)



(b)



(c)

Figure 3.8: (a) The anatomical model of diverse humerus shapes. (b) A partial humerus detected, and (c) no humerus detected. Replicated from El-Kwae et al. [38].

3.3 Thesis aim

The previous sections have identified the related work that has been performed on both computer aided diagnosis and medical image segmentation. This search revealed that there is no evidence of complete solutions to the problem of semi-automatic long-bone fracture detection. This section summarises the previous work and identifies its limitations, it establishes what has not been done before and what needs to be done, and also describes the aims of this thesis.

3.3.1 Summary of the previous research

The literature review revealed that in comparison to some areas of medical imaging, such as microcalcification identification in mammograms, very little research has been published on bone fracture detection. Sections 3.1 and 3.2 described all the relevant work that was found. To summarise, the CAD and segmentation literature that is specific to bones is:

- Detection of femur fractures using the NSA (Section 3.1.1)
- Detection of femur fractures using Gabor orientation maps (Section 3.1.1)
- Detection of osteoporosis from texture and fractal analysis (Section 3.1.2)
- Bone age estimation by model matching and classification (Section 3.1.3)
- Segmentation of cervical vertebrae using a generalised Hough Transform that searches the image for a previously defined template (Section 3.2.2)
- Arm bone segmentation using a prior shape and maximum-likelihood function (Section 3.2.4)
- Long-bone segmentation using a model created from statistical variations in anatomical data from diverse bone shapes (Section 3.2.5)

These methods all work with varying degrees of accuracy, but they also all suffer from some type of limitation. In most cases the first major limitation is that they were not

designed for long-bone fracture detection. However, the arm bone segmentation and long-bone segmentation methods appear to be insufficient.

3.3.2 Common limitations of the previous research

Amongst all the methods that were described in this chapter, three common limitations were identified. The first limitation was the requirement for finding an accurate model for many of the methods, before any analysis can be performed. This was necessary for the neck shaft angle calculation, bone age estimation, long-bone segmentation (including the arm fractures) and the vertebral segmentation. Some of these methods required particularly strict models, for example the arm fracture segmentation appeared to require a very accurate model to be manually created before matching could be performed.

Secondly, in some cases the models were limited and did not necessarily match well. An example of the poor detection produced by El Kwae's model is shown in Figure 3.8. Although not all authors showed these poor matches, it is highly likely that their methods suffered from similar problems. Some methods traded the accuracy with which they could match any one individual case for a better global detection, by creating a mean image from a large number of images that captured the natural anatomic variation.

The final common limitation was that the methods that utilised active contours, such as the neck shaft angle calculation and bone age estimation, required strict initial conditions to produce a good segmentation. Without good initial conditions the final contour does not match the object accurately. To determine the initial conditions it is assumed that manual setup is required. Active contour methods also perform better when used to segment tubular structures, like those examined in Section 3.2.3, but are not so successful for complex shapes like bones and joints. Accordingly, active contours are not utilised within this thesis.

3.3.3 What has not been done before

In addition to identifying the previous work that has been performed, the literature review also effectively identified what has not yet been achieved in the field of fracture detection in long-bones. Firstly, despite locating information about the various segmentation methods already described, there was no information about methods for automatically segmenting long-bones into their anatomic regions, as defined by the AO method in Section 2.5.1 and Figure 2.10. Secondly, there are no algorithms for detecting fractures within long-bones, other than the neck of femur as described in Section 3.1.1.

3.3.4 Thesis aims and goals

Based on the previous work discussed throughout this chapter one major goal was clear. A better long-bone fracture CAD method needed to be developed, to aid the radiologist in reducing the fracture miss rate by minimising the SOS effect, and subsequently improving patient treatment outcomes. As with other CAD systems for medical imaging, the radiologist does not necessarily want a complete system to detect fractures without any human intervention. A completely autonomous system would place all the responsibility of the diagnosis on this system, ultimately rendering the radiologist unnecessary. Instead, an algorithm that can highlight the regions that are of concern and should be looked at more carefully, possibly after the radiologist has already performed their preliminary diagnosis, would be of great value. This is similar to state of the art mammogram reading, where a computer is used to highlight areas of interest, rather than providing a diagnosis without any intervention or manual reading by the radiologist. In this way, the well trained eye of the human observer is supplemented with a computer system that can ensure that any regions missed on the initial reading are brought to the attention of that observer, before the final diagnosis is completed.

In order to produce a better CAD system for long-bone fracture detection, two major goals were identified:

1. To create a semi-automatic long-bone segmentation method to identify the different regions of a long-bone, so that the diaphyseal and epiphyseal segments could

be separated.

2. To create a semi-automatic long-bone fracture detection method that could identify fractures within the diaphyseal segment of the bone. The fracture detection algorithm should be able to detect all fractures within the diaphyseal segment with the smallest possible number of false negatives and false positives. That is, it should increase both the accuracy and reliability of detecting all long-bone fractures, and as a byproduct it should also ultimately reduce the fracture miss rate. Finally, the algorithm should perform the fracture detection with a minimal amount of user input, and in the shortest time possible.

Although it is desirable to detect all fractures within the diaphyseal segment, the primary objective is to detect the very subtle fractures that are not obvious to an untrained observer, and are more likely to be missed by a radiologist during reporting. It is possible that the fractures that are most obvious to humans are also the hardest for a CAD system to identify. As a result, the computer can add value to the detection process by complementing rather than replacing human experts. However, to achieve the second goal stated above, detection of both subtle and obvious fractures is attempted within this thesis. In addition, although Section 2.5.1 stated that long-bone fractures were chosen for initial fracture detection, hopefully this type of algorithm could eventually be used for detecting fractures in other anatomic regions, and eventually in all bones throughout the body.

The novel CAD algorithm for fracture identification developed in this thesis consists of four key components that are covered in the following chapters:

1. Extraction of the bone edges (Chapter 4)
2. Determination of global parameters that are used to approximate the pertinent bone edges (Chapter 5)
3. Long-bone diaphysis identification using the global parameters and a bone curvature based segmentation method (Chapter 6)
4. Highlighting the abnormal parts of the segmented region using gradient analysis (Chapter 7)